

## Photodissociation of Tetramethylene Sulfoxide at 193 and 248 nm in the Gas Phase

Fei Wu, Xirong Chen, and Brad R. Weiner\*

*Department of Chemistry and Chemical Physics Program, University of Puerto Rico, Box 23346 UPR Station, Rio Piedras, Puerto Rico 00931**Received: June 22, 1995; In Final Form: September 14, 1995*<sup>⊗</sup>

The 193 and 248 nm photodissociation of tetramethylene sulfoxide (TMSO) in the gas phase has been investigated by using laser spectroscopic techniques. The vibrational state distributions of the nascent SO( $X^3\Sigma^-$ ) photofragment following irradiation at 193 and 248 nm have been measured by using laser-induced fluorescence (LIF) spectroscopy on the  $B^3\Sigma^- - X^3\Sigma^-$  transition. These vibrational state distributions can be characterized as Boltzmann with vibrational temperatures of  $1250 \pm 60$  and  $1220 \pm 60$  K for the 193 and 248 nm photolyses, respectively. Assuming that the SO photofragment is produced in concert with a 1,4-tetramethylene diradical, the vibrational state distribution obtained in the 193 nm photolysis agrees well with an energy disposal model, in which the full reaction exoergicity is statistically partitioned among all the products' degrees of freedom. The quantum yield for SO( $X^3\Sigma^-$ ) production at 193 nm,  $\Phi_{SO}^{193} = 0.47 \pm 0.20$ , has been obtained by comparison with SO<sub>2</sub> photolysis. For the 248 nm photodissociation, the experimentally obtained vibrational state distribution can be best described by a variant statistical model assuming three-body fragmentation; *i.e.* the products are an SO fragment and two ethylene molecules. The quantum yield for SO( $X^3\Sigma^-$ ) production at 248 nm is  $\Phi_{SO}^{248} = 0.44 \pm 0.19$ . The OH photofragment has been detected during both the 193 and 248 nm photolyses of TMSO. The rotational state distributions of the OH( $X^2\Pi, v''=0$ ) fragment have been determined by LIF spectroscopy using the  $A^2\Sigma - X^2\Pi$  transition. The hydroxyl rotational temperatures can be characterized as  $600 \pm 50$  and  $510 \pm 40$  K following photolysis of TMSO at 193 and 248 nm, respectively. Mechanisms for the production of both SO and OH are discussed.

## Introduction

The partitioning of energy among the nascent photoproducts following photoactivation of polyatomic molecules remains one of the most powerful techniques for unraveling their detailed photodissociation dynamics.<sup>1</sup> In small polyatomic systems, *i.e.* triatomic and tetraatomic, photofragmentation pathways are often limited, and therefore the photodissociation dynamics can be investigated in great detail. Large molecular systems remain a complicated problem, owing to the possibility of multiple product channels and the large number of degrees of freedom available for energy partitioning. Among the more interesting cases are those polyatomic fragmentation reactions that undergo multiple bond cleavage, raising the question of whether the photodissociation occurs in a sequential or concerted manner. For the photoelimination of diatomic fragments from a cyclic species, the measurement of the internal energy distribution of the resulting diatomic photofragment has been used in elucidating the dissociation mechanism. For example, measurements of the energy disposal to the carbon monoxide fragment have revealed mechanistic information about the thermal and photochemical dissociations of several saturated and unsaturated cyclic ketones.<sup>2–6</sup>

The photochemistry of tetramethylene sulfoxide (TMSO) has been studied in flash photolysis experiments by using gas chromatography in conjunction with mass spectrometry to measure the stable hydrocarbon product distributions.<sup>7,8</sup> Dorer and Salomon reported that flash photolysis of gas-phase TMSO in the wavelength region 202–228 nm produced ethylene,

propylene, cyclopropane, 1-butene, cyclobutane, and a small amount of butadiene.<sup>7</sup> They found that the product distributions depended on the photolysis wavelength. Triplet-sensitized (Hg, 253.7 nm) decomposition of TMSO in the gas phase produced only ethylene and propylene. The results were interpreted in terms of a mechanism which involves initial rupture of a C–S bond to form a diradical intermediate. Scala *et al.* studied the gas-phase photolysis of TMSO at 147 nm by also measuring the hydrocarbon product distribution.<sup>8</sup> They concluded that the predominant dissociation channel involves the formation of ethylene and C<sub>2</sub>H<sub>4</sub>SO by  $\beta$ -cleavage of the initially produced diradical. To our knowledge, no experiments have been carried out to directly probe the nascent products following the photodissociation of TMSO.

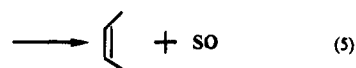
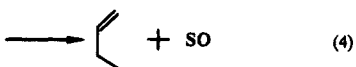
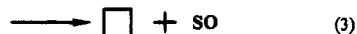
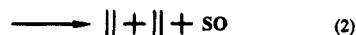
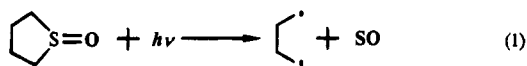
Jug *et al.* studied the photochemical decomposition of TMSO by using the semiempirical molecular orbital method, SINDO1, to calculate the relevant singlet and low-lying triplet potential energy hypersurfaces with limited configuration interaction.<sup>9</sup> These authors favored concerted multiple bond cleavages of the parent TMSO as the operative mechanism to form the main reaction products: ethylene, cyclobutane, propene, and 1-butene. This conclusion differs from previous assertions,<sup>7,8</sup> where the  $\alpha$ -cleavage is the primary photochemical event.

In this work, we probe the nascent SO( $X^3\Sigma^-$ ) photofragment following 193 and 248 nm photolysis of TMSO by using laser-induced fluorescence (LIF) spectroscopy on the  $B^3\Sigma^- - X^3\Sigma^-$  transition. The relative vibrational state distributions, as well as the quantum yields, of the nascent SO( $X^3\Sigma^-$ ) photofragment measured following 193 and 248 nm photolyses are reported. In the ultraviolet photodissociation of tetramethylene sulfoxide,

\* To whom correspondence should be addressed.

⊗ Abstract published in *Advance ACS Abstracts*, November 1, 1995.

the energetically allowed reaction channels to produce the nascent SO diatomic photofragment are



We have also detected the OH photofragment following the photolysis of TMSO at 193 and 248 nm. The rotational state distribution of OH( $X^2\Pi, v''=0$ ) fragment has been determined by LIF spectroscopy on the  $A^2\Sigma, v' = 1 - X^2\Pi, v'' = 0$  transition. These measurements provide direct information about the photodissociation process and help us to elucidate the detailed photodissociation dynamics of TMSO at 193 and 248 nm.

### Experimental Section

The experimental apparatus used in these studies has been described previously.<sup>10,11</sup> In brief, the TMSO is introduced into a stainless steel reaction chamber by flowing helium buffer gas through a glass trap which contains the pure compound. The stainless steel chamber is equipped with extension arms (to reduce scattered light) through which the lasers are introduced through fused silica windows. TMSO partial pressures ( $7 \pm 3$  mTorr) are limited by the room temperature vapor pressure of the compound. All partial and total pressures are measured at the exit of the chamber by a calibrated capacitance manometer. Helium buffer gas (300 mTorr) was flowed onto the windows to prevent buildup of heterogeneous photolysis products. The total pressure in the reaction chamber was 400–500 mTorr.

Tetramethylene sulfoxide is photolyzed by either the 193 nm (ArF, 3–6 mJ/cm<sup>2</sup>) or 248 nm (KrF, 12–18 mJ/cm<sup>2</sup>) output of an excimer laser (Lambda Physik LPX205). Sulfur monoxide photofragments are monitored by LIF on the  $B^3\Sigma^- - X^3\Sigma^-$  transition in the 237–295 nm region of the spectrum. OH photofragments are also monitored by LIF on the  $A^2\Sigma - X^2\Pi$  transition in the 280–295 nm region. The probe laser light is generated by frequency-doubling ( $\beta$ -BaB<sub>2</sub>O<sub>4</sub> crystal) the output of a Lambda Physik LPD3002 tunable dye laser, which is pumped by a Lambda Physik LPX205 excimer laser operating on the XeCl transition at 308 nm. Three dyes, Coumarin 480, 503, and 540A, are used in order to cover the entire frequency region of the SO and OH signal. The two laser beams, photolysis and probe, are collinearly counterpropagated along the entire length of the cell to ensure maximum overlap in the center of the reaction chamber.

Fluorescence is viewed at 90° relative to the laser beam axis by a high gain photomultiplier tube (PMT) through two long-pass filters (Schott WG280 and 295). The output of the PMT is processed by a gated integrator (SRS Model SR250) and digitizer (SRS Model SR245) and sent to a microcomputer for display, storage, and analysis. The delay time between photolysis and probe lasers is controlled by a digital delay pulse

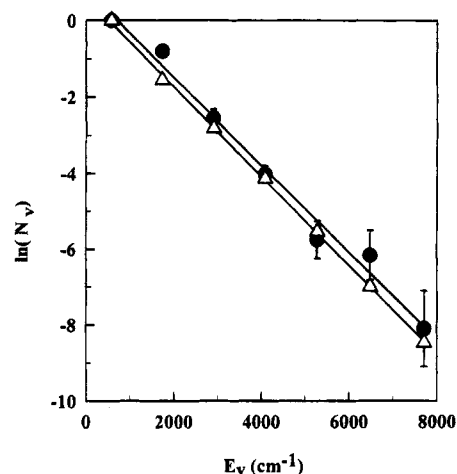


**Figure 1.** Experimental and calculated  $\ln N_v$  vs vibrational energy plots for  $\text{SO}(X^3\Sigma^-)$  vibrational state distribution following 193 nm photolysis of TMSO: ●, experimental data ( $T_{\text{vib}} = 1250 \pm 60$  K); △, results obtained by application of eq 7 to eq 1. See text for further discussion.

generator (SRS Model DG535) and fixed between 100 and 2000 ns. For a fixed delay time between photolysis and probe laser, the frequency-doubled output of the dye laser is scanned while collecting the total fluorescence signal to obtain a nascent excitation spectrum. Data were collected at 30 Hz, with each point representing the average of 10 shots. The LIF intensity is found to be a linear function of the dye laser power, and signals taken over a large wavelength region were normalized to the dye laser power. For photolysis at either 193 or 248 nm, a linear dependence on pump laser fluence was observed. This result indicates that the ground state SO is produced by a single-photon process.

TMSO (Lancaster, 97%) was distilled under reduced pressure and subjected to three freeze–pump–thaw cycles prior to use. Sulfur dioxide and helium (Air Products, 99.9%) were used without further purification as a calibrant and buffer gas, respectively, in the quantum yield measurements.

### Results

LIF signals, assignable to the  $\text{SO}(B^3\Sigma^- - X^3\Sigma^-)$  transition, have been obtained under collision-free conditions, where the total pressure in the reaction chamber is 500 mTorr and the probe delay time is less than 100 ns. To avoid the interference of the emission induced by the photolysis laser, LIF spectra were recorded at longer probe delay times (*i.e.* 2  $\mu\text{s}$ ). Under these conditions, *ca.* 10 hard-sphere collisions, the vibrational state distribution of the SO photofragment remains unrelaxed even though rotational populations are partially relaxed.<sup>12</sup> The relative vibrational state populations of  $\text{SO}(X^3\Sigma^-)$ ,  $N_v$ , were obtained by integrating the areas under the  $(1, v'')$  vibronic transitions (where  $v'' = 0-6$ ) and correcting the integrated areas by the appropriate Franck–Condon factor.<sup>13</sup> Experimental distributions of the nascent  $\text{SO}(X^3\Sigma^-)$  photofragment can be characterized by a vibrational temperature of  $1250 \pm 60$  and  $1220 \pm 60$  K following the 193 and 248 nm photolyses, respectively. Vibrational temperatures are obtained from a  $\ln(N_v)$  vs SO vibrational energy content ( $E_{\text{vib}}$ ) plot as shown in Figures 1 and 2.

We have attempted to measure nascent SO rotational state distributions following the photodissociation of TMSO at both wavelengths. In both cases, we are not able to do so because of a large emission feature following the photolysis laser pulse. Partially relaxed rotational state distributions have been mea-

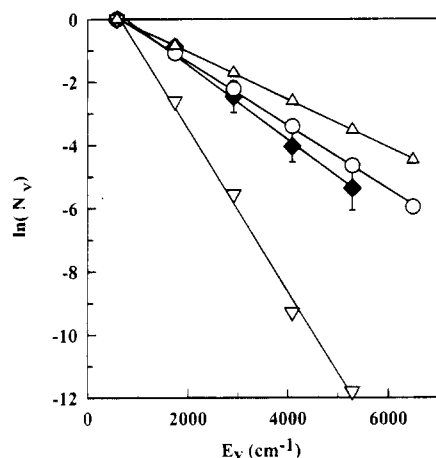


**Figure 2.** Experimental and calculated  $\ln N_v$  vs vibrational energy plots for  $\text{SO}(\text{X}^3\Sigma^-)$  vibrational state distribution following 248 nm photolysis of TMSO:  $\blacklozenge$ , experimental data ( $T_{\text{vib}} = 1220 \pm 60$  K);  $\nabla$ , results obtained by application of eq 7 to eq 1;  $\triangle$ , results obtained by application of eq 7 to eq 3;  $\circ$ , results obtained by application of eq 8 to eq 2. See text for further discussion.

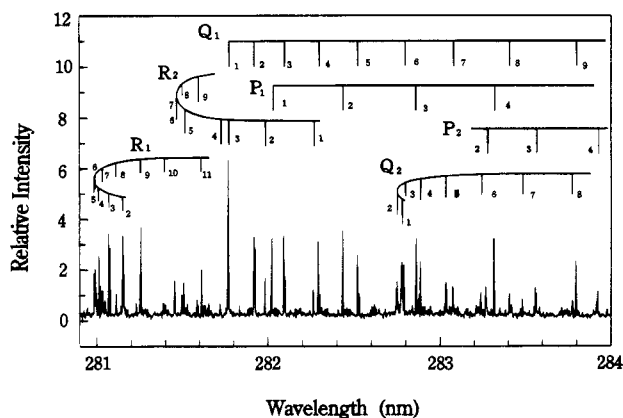


**Figure 3.** LIF spectrum of  $\text{OH}(\text{A}^2\Sigma, v'=1-\text{X}^2\Pi, v''=0)$  resulting from the 193 nm photolysis of 0.007 Torr of TMSO in 0.35 Torr of He buffer gas. The delay time between the lasers was 0.2  $\mu\text{s}$ .

sured for several vibrational bands of the  $\text{SO}(\text{B}-\text{X})$  transition, but we have not used these data in the analysis due to the scrambling of the information content by collisions.

LIF spectral lines appear in the region 280–295 nm, which cannot be assigned to the  $\text{SO}(\text{B}-\text{X})$  transition. The lines, which appear following TMSO photolysis at both 193 and 248 nm under collision-free conditions, are assignable to the  $\text{OH}(\text{A}^2\Sigma, v'=1-\text{X}^2\Pi, v''=0)$  transition, as shown in Figure 3. Assignments were made on the basis of the tabulated results of Dieke and Crosswhite.<sup>14</sup> These spectra were collected under low probe laser fluence (*ca.* 50  $\mu\text{J}/\text{pulse}$ ) conditions to avoid saturation of the  $\text{OH}(\text{A}-\text{X})$  transition. Under these conditions, the spectral lines associated with the  $\text{SO}(\text{B}-\text{X})$  transition disappear. The rotational temperatures of the nascent  $\text{OH}(\text{X}^2\Pi, v''=0)$  photofragment are found to be  $600 \pm 50$  and  $510 \pm 40$  K following 193 and 248 nm photolysis of TMSO, respectively. No other vibrational states, *i.e.*  $v'' \geq 1$ , of the  $\text{OH}(\text{X}^2\Pi)$  photofragment are observed.

We have measured the quantum yields at both photolysis wavelengths of  $\text{SO}(\text{X}^3\Sigma^-)$  production, which may provide insight into the photodissociation mechanism of TMSO. In our experiments, the LIF signal of a given rovibronic transition, corresponding to  $\text{SO}(\text{X}^3\Sigma^-, v''=2, N''=11)$  vibrational state, was used to measure the quantum yield. We recorded the LIF signal intensities originating from  $\text{SO}(\text{X}^3\Sigma^-)$  following the photodissociation of TMSO and  $\text{SO}_2$  under identical conditions except

for photolysis laser fluence (3.5  $\text{mJ}/\text{cm}^2$  at 193 nm and 14  $\text{mJ}/\text{cm}^2$  at 248 nm). The relative  $\text{SO}(\text{X}^3\Sigma^-)$  quantum yield,  $\phi$ , was derived as follows:

$$\phi = I_{\text{SO}(\text{I})} / (\sigma P(v'') P_{\text{laser}}) \quad (6)$$

where  $\sigma$  is the absorption cross section of the parent molecule at the corresponding photolysis wavelength,  $P(v'')$  is the fractional nascent population in the vibrational state of  $\text{SO}(\text{X}^3\Sigma^-, v''=2)$ , and  $P_{\text{laser}}$  is the fluence of the photolysis laser. Due to the uncertainty of the vapor pressure of TMSO, a precise measurement of the absorption cross section is difficult. We estimate the vapor pressure of TMSO to be  $7 \pm 3$  mTorr at room temperature. From the UV absorption spectrum of TMSO in the gas phase, the absorption cross sections are found to be  $\sigma_{193} = (5.3 \pm 2.3) \times 10^{-17} \text{ cm}^2 \text{ molecule}^{-1}$  and  $\sigma_{248} = (4.8 \pm 2.0) \times 10^{-19} \text{ cm}^2 \text{ molecule}^{-1}$ , in good agreement with previous measurements.<sup>7</sup> These cross sections are used to calculate the quantum yields of  $\text{SO}(\text{X}^3\Sigma^-)$  from the 193 and 248 nm photolyses of TMSO. Since the  $\text{SO}(\text{X}^3\Sigma^-)$  production is greater than 99.5% from the 193 nm photolysis of  $\text{SO}_2$ ,<sup>15</sup> we assume it to be unity. By comparing  $\phi$  from the photolysis of TMSO at both 193 and 248 nm with the  $\phi$  value from the photolysis of  $\text{SO}_2$  at 193 nm, the absolute quantum yield,  $\Phi$ , of  $\text{SO}(\text{X}^3\Sigma^-)$  from TMSO was obtained:

$$\Phi_{\text{SO}}^{193} = \phi_{193\text{nm}}^{\text{TMSO}} / \phi_{193\text{nm}}^{\text{SO}_2} = 0.47 \pm 0.20$$

$$\Phi_{\text{SO}}^{248} = \phi_{248\text{nm}}^{\text{TMSO}} / \phi_{193\text{nm}}^{\text{SO}_2} = 0.44 \pm 0.19$$

The errors arise primarily from the uncertainty of the vapor pressure of TMSO.

## Discussion

Our results indicate that TMSO undergoes photoelimination of either an SO or OH molecule following irradiation at 193 or 248 nm. The gas-phase absorption spectrum of TMSO at room temperature that we observe is structureless with the onset around 250 nm. The absorption cross section at 248 nm is small compared with that at 193 nm. Absorption of a 193 nm photon is believed to lead to an excited singlet state.<sup>9</sup> It is possible that, by absorbing a 248 nm photon, the TMSO molecule undergoes a direct excitation to a triplet state.<sup>9</sup> Quantum yield measurements on the  $\text{SO}(\text{X}^3\Sigma^-)$  species account for approximately half of the photophysical processes at both wavelengths. The dissociation to OH and other products may account for the remaining processes due to photoactivation, but has not been quantified here.

The nascent vibrational state distribution of the SO photofragment resulting from 193 nm photolysis of TMSO can be characterized by a vibrational temperature as shown in Figure 1. Some insight regarding the mechanism of SO photoelimination can be obtained by comparing the experimental data with that anticipated on the basis of an assumed model. There are five energetically allowed dissociation reaction channels which produce the nascent SO photofragment (see eqs 1–5). An energy level diagram for the reactions represented by eqs 1–3 is shown in Figure 4. If SO is formed together with an unstable intermediate, *i.e.* a diradical (eq 1), the maximum energy available is  $E_{\lambda}$ , where photoactivation is carried out at wavelength,  $\lambda$ . If the sulfur monoxide remains strongly coupled to the diradical until stable products are formed or if the dissociation is a single-step, concerted process yielding the SO photofragment plus other stable product(s) (*e.g.* eqs 2 and 3), then the corresponding available energies are  $E'_{\lambda}$  or  $E''_{\lambda}$  depending

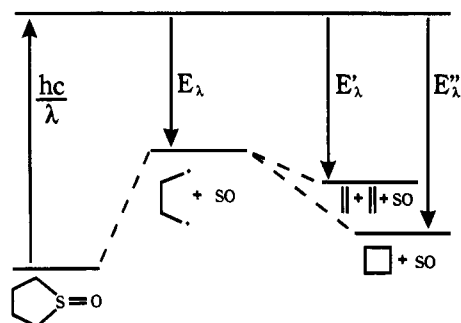


Figure 4. Schematic energy level diagram for reactions represented by eqs 1–3.

TABLE 1: Energy Available to the Products following Photodissociation of TMSO (cf. Figure 4)

$\lambda$ (nm)	$E_\lambda$ , kcal/mol	$E'_\lambda$ , kcal/mol	$E''_\lambda$ , kcal/mol
193	47	83	102
248	14	51	69

on the reaction channel. These energies can be evaluated using thermochemical estimation methods,<sup>16</sup> and the results are given in Table I.

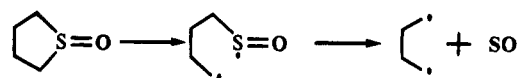
For a given choice of available energy and relative products, the nascent vibrational state distribution can be predicted using a statistical energy disposal model developed by Bogan *et al.*<sup>17</sup> and Rosenfeld and co-workers.<sup>18</sup> The probability,  $f(\epsilon, E)$ , of forming an SO photofragment with vibrational energy,  $\epsilon$ , for a given available energy,  $E$ , is given by

$$f(\epsilon, E) = \frac{N_{SO}(\epsilon) \int_{E_t=0}^{E-\epsilon} P_r(E-\epsilon-E_t) \sqrt{E_t} dE_t}{\sum_{\epsilon=0}^E N_{SO}(\epsilon) \int_{E_t=0}^{E-\epsilon} P_r(E-\epsilon-E_t) \sqrt{E_t} dE_t} \quad (7)$$

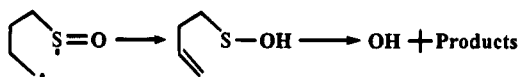
Here  $N_{SO}(\epsilon)$  is the vibrational density of states of SO at vibrational energy,  $\epsilon$ , which can be calculated from the harmonic oscillator approximation.  $P_r(E-\epsilon-E_t)$  is the total number of states corresponding to the vibrational and all relative rotational degrees of freedom of the other fragment(s) at energy  $E - \epsilon - E_t$ . For the three-body case, *i.e.* eq 2, a more detailed description of the model is given below.  $P_r(E)$  is calculated by using the Whitten–Rabinovitch semiclassical algorithm.<sup>19</sup> The 30 fundamental vibrational frequencies of the 1,4-tetramethylene diradical used in calculating  $P_r(E)$  are taken from the result of an *ab initio* calculation of singlet tetramethylene.<sup>20</sup>  $\sqrt{E_t}$  is proportional to the one-dimensional translational density of states<sup>21</sup> at energy  $E_t$ . The SO vibrational state distribution, calculated by using eq 7 based on the full reaction exoergicity available to eq 1, is plotted in Figure 1. We find that the calculated SO vibrational state distribution is in excellent agreement with the 193 nm data. Other available energies corresponding to other reaction channels do not resemble the experimentally determined SO vibrational energy distribution. This model supports the hypothesis that the primary nascent products in the 193 nm photodissociation of TMSO are the 1,4-tetramethylene diradical and the ground state SO fragment.

The remaining question is whether the 193 photodissociation of TMSO proceeds, via a stepwise bond cleavage process to produce a 1,5-tetramethylenesulfinyl diradical intermediate, or a concerted process in which both C–S bonds are simultaneously broken to give tetramethylene diradical and SO (see Scheme 1). Since the SO vibrational state distribution that we measured here is statistical in nature, it is difficult to answer this question conclusively. A detailed nascent rotational

#### SCHEME 1



#### SCHEME 2



distribution, which we were unable to measure, would be useful data in helping to conclude whether this process proceeds via a stepwise or concerted mechanism.

One possible mechanism for the formation of OH, consistent with our detection of the radical in only the ground vibrational state, is shown in Scheme 2. In this type of mechanism, there would be time for a complete randomization of the energy within the intermediates, so that one might expect the OH fragment to have equilibrated rotational and vibrational temperatures. If the vibrational temperature of OH( $X^2\Pi$ ) was 600 K, the population of OH( $v''=1$ ) would be approximately  $10^{-5}$  times less than OH( $v''=0$ ). Thus, we would not expect to see it. An alternative mechanism that is not consistent with the observed data is the concerted elimination of the hydroxyl radical involving the  $\alpha$ -hydrogen of TMSO or the intermediate 1,5-tetramethylenesulfinyl diradical species. This four-center reaction might be expected to eliminate a vibrationally excited OH fragment, by analogy with the hydrogen halide elimination in halogenated alkanes.<sup>22</sup> We have thus ruled out this type of elimination reaction.

Quantum yield measurements, in conjunction with our vibrational energy partitioning results, indicate that 47% of the photoactivated TMSO at 193 nm dissociate to form the 1,4-tetramethylene diradical and ground state SO. The remaining photoactivated parent molecules undergo either non-SO-producing reactions, including the OH elimination reaction, or produce SO in other low-lying electronic states. We see no increase in the SO signal as a function of increased time delay between the two lasers, which would be consistent with photoproduction of SO in other electronic states, followed by relaxation to the ground state. We conclude that all the sulfur monoxide formed is produced in the ground  $X^3\Sigma^-$  state.

The tetramethylene fragment can undergo further cyclization and/or fragmentation to produce cyclobutane and/or ethylene, respectively. *Ab initio* calculations by Doubleday show that the ratio of the rate constants of cyclization versus fragmentation depend on the vibrational temperature of the tetramethylene fragment.<sup>20</sup> According to our experimental results, the vibrational temperature of the SO fragment is *ca.* 1200 K. Since the available energy is randomly partitioned among all the products' degrees of freedom in our model, we can assume the vibrational temperature of the tetramethylene fragment to be equal to that of the SO photofragment. The *ab initio* calculations show that the ratio of cyclization versus fragmentation of tetramethylene at 1200 K is  $k_{cyc}/k_{frag} = 0.27$ . This ratio is consistent with the results of flash photolysis experiments. The experimentally measured product ratio of cyclobutane to ethylene is about 0.3 when the photolysis wavelength range is between 202 and 225 nm.<sup>7</sup>

The vibrational state distribution of the SO( $X^3\Sigma^-$ ) photofragment following 248 nm photolysis of TMSO can also be characterized as statistical, with a vibrational temperature of  $1220 \pm 60$  K. The OH fragment has been once again observed, with population in only the ground vibrational state. As shown in Scheme 1, the diradical intermediate undergoes a two-body fragmentation to produce SO and tetramethylene. Application

of eq 7 to eq 1 ( $\lambda = 248$  nm) yields a calculated vibrational state distribution of the SO photofragment that is much colder than the experimentally determined results (see Figure 2), even though the available energy,  $E_{248} = 14$  kcal/mol, is the full exoergicity (cf. Table 1). The formation of the 1,4-tetramethylene diradical and SO photofragment can thus be ruled out in the context of our assumed model. Another possibility is the simultaneous formation of the two ethylene fragments with the production of SO, *i.e.* a three-body fragmentation, as shown in eq 2. A variant statistical model for three-body fragmentation is employed to calculate the SO vibrational state distribution for eq 2.<sup>23</sup> In this model, the probability,  $f(\epsilon, E)$ , of forming the SO photofragment with vibrational energy,  $\epsilon$ , for a given available energy,  $E$ , is given by

$$f(\epsilon, E) = \frac{N_{\text{SO}}(\epsilon) \int_{E_t=0}^{E-\epsilon} w(E-\epsilon-E_t)(E_t)^2 dE_t}{\sum_{\epsilon=0}^E N_{\text{SO}}(\epsilon) \int_{E_t=0}^{E-\epsilon} (E-\epsilon-E_t)(E_t)^2 dE_t} \quad (8)$$

$w(E-\epsilon-E_t)$  is the total number of states corresponding to the vibrational and all relative rotational degrees of freedom of two ethylene molecules at energy  $E - \epsilon - E_t$  and is given by

$$w(E-\epsilon-E_t-e) = \int_{e=0}^{E-\epsilon-E_t} P_t(E-\epsilon-E_t-e) P_r'(e) de \quad (9)$$

$$P_r'(e) = dP(e)/de \quad (10)$$

$P_t(e)$  is the total number of states corresponding to the vibrational and all relative rotational degrees of freedom of an ethylene at energy  $e$ .  $(E_t)^2$  is proportional to the translational density of states for a three-body dissociation at translational energy,  $E_t$ .<sup>24</sup> We find that the calculated vibrational state distribution of the SO photofragment is consistent with the experimentally determined distribution if the available energy is equal to reaction exoergicity (see Figure 2).

Equation 3, which produces cyclobutane and the SO photofragment, is also a possible reaction channel. By applying eq 7 to eq 3, we find that the calculated SO vibrational state distribution is much hotter than the experimental data when the available energy is equal to the reaction exoergicity,  $E = 71$  kcal/mol. The comparison of the calculated SO vibrational state distributions on eqs 1–3 and the experimentally determined SO vibrational state distribution in the 248 nm photolysis of TMSO is shown in Figure 2. Applications of eq 7 to the reactions shown in eqs 4 and 5 would give results that disagree more strongly than those from eq 3. These results indicate that the 248 nm photolysis of TMSO is consistent with the three-body fragmentation of the diradical intermediate to produce two ethylene molecules and an SO photofragment, if a statistical energy disposal energy model is assumed.

On first inspection, the 193 and 248 nm photolyses of TMSO seem similar. Irradiation at either wavelength produces about the same quantum yield of ground state sulfur monoxide, and both photolyses yield the hydroxyl radical at similar rotational temperatures. However, when the experimental results are compared with a physical model for the dissociation, the two photolysis wavelengths seem to lead to different photochemical pathways. Upon 193 nm irradiation of TMSO, a C–S bond rupture occurs followed by the production of the tetramethylene diradical and the SO fragment. Based on our model, the same 1,5-tetramethylenesulfinyl diradical intermediate is produced after 248 nm irradiation of TMSO, but now the SO moiety is produced along with the two ethylene molecules. One possible explanation of this difference is that the 1,5-tetramethylene-

sulfinyl diradical intermediate is produced in two different electronic states, *i.e.* singlet and triplet, and therefore has different dissociation pathways. This explanation is consistent with the small absorption cross section of TMSO at 248 nm. Namely, 248 nm irradiation generates <sup>3</sup>TMSO directly, which subsequently dissociates on a triplet surface. This explanation is consistent with the previous product study results,<sup>7</sup> where cyclobutane is only formed at the shorter wavelengths ( $\lambda < 225$  nm), corresponding to the production of the tetramethylene diradical on the singlet surface.

## Summary and Conclusions

Vibrational state population distributions and the quantum yields of the nascent  $\text{SO}(X^3\Sigma^-)$  photofragment from the 193 and 248 nm photodissociation of TMSO in the gas phase have been measured by laser-induced fluorescence spectroscopy. The OH photofragment has been detected during the 193 and 248 nm photolysis of TMSO under collision-free conditions. In both cases, the photolysis may produce a 1,5-tetramethylenesulfinyl diradical intermediate. The vibrational state distribution of the  $\text{SO}(X^3\Sigma^-)$  photofragment following 193 nm photolysis is compared with the distributions calculated by using a statistical model assuming the products to be a 1,4-tetramethylene diradical and SO. When the full reaction exoergicity is statistically partitioned among all the products' degrees of freedom at 193 nm photolysis, a strong agreement between the experimental results and the model is obtained. For the 248 nm photodissociation, the experimentally obtained vibrational state distribution can be best described by a variant statistical model for three-body fragmentation assuming the products to be an SO fragment and two ethylene molecules.

**Acknowledgment.** We acknowledge the generous support of this project by the Air Force Office of Scientific Research through Grants F49620-92-5-0406 and F49620-93-1-0110. The experiments performed here were done in conjunction with the Puerto Rico Laser and Spectroscopy Facility at the University of Puerto Rico, under the auspices of the NSF-EPSCoR and NIH-RCMI programs. The authors kindly acknowledge Dr. John A. Soderquist for helpful discussions. The authors also thank Ms. Cyntia Espada and Ms. Yazmín Pedrogo for taking the absorption spectra of TMSO and Mr. Rudy Rivera for his mechanical assistance.

## References and Notes

- (1) Bersohn, R. In *Molecular Photodissociation Dynamics*; Ashfold, M. N. R., Baggott, J. G., Eds.; Royal Society of Chemistry: London, 1987; pp 1–30.
- (2) Jimenez, R.; Kable, S. H.; Loison, J.-C.; Simpson, C. J. S. M.; Adam, W.; Houston, P. L. *J. Phys. Chem.* **1992**, *96*, 4188.
- (3) (a) Buxton, J. P.; Simpson, C. J. S. M. *Chem. Phys.* **1986**, *105*, 307. (b) Simpson, C. J. S. M.; Price, J.; Holmes, G.; Adam, W.; Martin, H.-D.; Bish, S. J. *Am. Chem. Soc.* **1990**, *112*, 5089.
- (4) Prather, K. A.; Rosenfeld, R. N. *J. Phys. Chem.* **1991**, *95*, 6544.
- (5) Sonobe, B. I.; Fletcher, T. R.; Rosenfeld, R. N. *J. Am. Chem. Soc.* **1984**, *106*, 4325, 5800.
- (6) Trentelman, K. A.; Moss, D. B.; Kable, S. H.; Houston, P. L. *J. Phys. Chem.* **1990**, *94*, 3031.
- (7) Dorer, F. H.; Salomon, K. E. *J. Phys. Chem.* **1980**, *84*, 1302.
- (8) Scala, A. A.; Colon, I.; Rourke, W. *J. Phys. Chem.* **1981**, *85*, 3603.
- (9) Jug, K.; Neumann, F.; Schluff, H.-P. *J. Org. Chem.* **1993**, *58*, 6634.
- (10) Chen, X.; Asmar, F.; Wang, H.; Weiner, B. R. *J. Phys. Chem.* **1991**, *95*, 6415.
- (11) Barnhard, K. I.; Santiago, A.; He, M.; Asmar, F.; Weiner, B. R. *Chem. Phys. Lett.* **1991**, *178*, 150.
- (12) Wang, H.; Chen, X.; Weiner, B. R. *J. Phys. Chem.* **1993**, *97*, 12260.
- (13) Smith, W. H.; Liszt, H. S. *J. Quant. Spectrosc. Radiat. Transfer* **1971**, *11*, 45.

- (14) Dieke, G. H.; Crosswhite, H. M. *J. Quant. Spectrosc. Radiat. Transfer* **1962**, 2, 97.
- (15) Kanamori, H.; Tiemann, E.; Hirota, E. *J. Chem. Phys.* **1988**, 89, 621.
- (16) Benson, S. W. *Thermochemical Kinetics*; Wiley-Interscience: New York, 1976.
- (17) Bogan, D. J.; Setser, D. W. *J. Chem. Phys.* **1976**, 64, 586.
- (18) Rosenfeld, R. N.; Weiner, B. *J. Am. Chem. Soc.* **1983**, 105, 3485.
- (19) Whitten, G. Z.; Rabinovitch, B. S. *J. Chem. Phys.* **1964**, 41, 1883.
- (20) Doubleday, C. *J. Am. Chem. Soc.* **1993**, 115, 11968.
- (21) Kinsey, J. L. *J. Chem. Phys.* **1971**, 54, 1206.
- (22) Arunan, E.; Wategaonkar, S. J.; Setser, D. W. *J. Phys. Chem.* **1991**, 95, 1539 and references therein.
- (23) Weiner, B. R.; Rosenfeld, R. N. *J. Phys. Chem.* **1986**, 90, 4037.
- (24) Berry, M. J. *Chem. Phys. Lett.* **1974**, 29, 323, 329.

JP951768M